ZTF 18aaqeasu (SN 2018byg): A Massive Helium-shell Double Detonation on a Sub-Chandrasekhar Mass White Dwarf

Kishalay De,[1] Mansi M. Kasliwal,[1] Abigail Polin,[2,3] Peter E. Nugent,[2,3] Lars Bildsten,[4,5] Scott M. Adams,[1] Eric C. Bellm,[6] Nadia Blagorodnova,[1] Kevin B. Burdge,[1] Christopher Cannella,[1] S. Bradley Cenko,[7,8] Richard G. Dekany,[9] Michael Feeney,[9] David Hale,[9] U. Christoffer Fremling,[1] Matthew J. Graham,[1] Anna Y. Q. Ho,[1] Jacob E. Jencson,[1] S. R. Kulkarni,[1] Russ R. Laher,[10] Frank J. Masci,[10] Adam A. Miller,[11,12] Maria T. Patterson,[6] Umaa Rebbapragada,[13] Reed L. Riddle,[9] David L. Shupe,[10] and Roger M. Smith[9]

[1] Cahill Center for Astrophysics, California Institute of Technology, 1200 E. California Blvd. Pasadena, CA 91125, USA.
[2] Department of Astronomy, University of California, Berkeley, CA, 94720-3411, USA.
[3] Lawrence Berkeley National Laboratory, Berkeley, California 94720, USA.
[4] Department of Physics, University of California, Santa Barbara, CA 93106, USA.
[5] Kavli Institute for Theoretical Physics, University of California, Santa Barbara, CA 93106, USA.
[6] DIRAC Institute, Department of Astronomy, University of Washington, 3910 15th Avenue NE, Seattle, WA 98195, USA
[7] Astrophysics Science Division, NASA Goddard Space Flight Center, Mail Code 661, Greenbelt, MD 20771, USA.
[8] Joint Space-Science Institute, University of Maryland, College Park, MD 20742, USA.
[9] Caltech Optical Observatories, California Institute of Technology, Pasadena, CA 91125, USA
[10] IPAC, California Institute of Technology, 1200 E. California Blvd, Pasadena, CA 91125, USA
[11] Center for Interdisciplinary Exploration and Research in Astrophysics (CIERA) and Department of Physics and Astronomy, Northwestern University, 2145 Sheridan Road, Evanston, IL 60208, USA
[12] The Adler Planetarium, Chicago, IL 60605, USA
[13] Jet Propulsion Laboratory, California Institute of Technology, Pasadena, CA 91109, USA

ABSTRACT

The detonation of a helium shell on a white dwarf has been proposed as a possible explosion triggering mechanism for Type Ia supernovae. Here, we report ZTF 18aaqeasu (SN 2018byg/ATLAS 18pqq), a peculiar Type I supernova, consistent with being a helium-shell double-detonation. With a rise time of ≈ 18 days from explosion, the transient reached a peak absolute magnitude of $M_R \approx -18.2$ mag, exhibiting a light curve akin to sub-luminous SN 1991bg-like Type Ia supernovae, albeit with an unusually steep increase in brightness within a week from explosion. Spectra taken near peak light exhibit prominent Si absorption features together with an unusually red color ($g - r \approx 2$ mag) arising from nearly complete line blanketing of flux blue-wards of 5000 Å. This behavior is unlike any previously observed thermonuclear transient. Nebular phase spectra taken at and after ≈ 30 days from peak light reveal evidence of a thermonuclear detonation event dominated by Fe-group nucleosynthesis. We show that the peculiar properties of ZTF 18aaqeasu are consistent with the detonation of a massive ($\approx 0.15\,M_\odot$) helium shell on a sub-Chandrasekhar mass ($\approx 0.75\,M_\odot$) white dwarf after including mixing of $\approx 0.2\,M_\odot$ of material in the outer ejecta. These observations provide evidence of a likely rare class of thermonuclear supernovae arising from detonations of massive helium shells.

Keywords: supernovae: general — supernovae: individual (SN 2018byg) — surveys — white dwarfs

1. INTRODUCTION

Corresponding author: Kishalay De
kde@astro.caltech.edu

In the double-detonation model for Type Ia supernovae (SNe), the explosive detonation of a helium (He) shell on the surface of a sub-Chandrasekhar mass white dwarf (WD) triggers a detonation in the core of the WD, leading to an explosion of the entire star (Nomoto 1980, 1982a,b; Woosley et al. 1986; Woosley & Weaver 1994;

Livne & Arnett 1995). Several key issues in this mechanism have been studied in recent years, including the conditions for the detonation of the He shell (that is accreted from a He-rich companion) and if the detonation in the shell can trigger a detonation in the underlying CO core (Bildsten et al. 2007; Fink et al. 2007, 2010; Sim et al. 2010; Shen & Bildsten 2014). These studies have generally concluded that detonations in the shell are triggered for He shell masses larger than $\sim 0.01\,M_\odot$, while at the same time inevitably leading to a detonation of the core (Bildsten et al. 2007; Fink et al. 2010; Shen et al. 2010; Shen & Moore 2014).

Consequently, several studies have also explored the observational signatures of these events and if they are consistent with observed diversity of Type Ia SNe (Kromer et al. 2010; Sim et al. 2010; Woosley & Kasen 2011; Polin et al. 2018). While simulations of the double detonation scenario in bare sub-Chandrasekhar mass CO WDs (i.e. without including the effects of the overlying He shell) have found that these explosions are capable of reproducing the observed diversity of Type Ia SNe (Sim et al. 2010; Shen et al. 2018), the results are quite different when including the ashes of the overlying He shell (rich in He burning products) in the radiative transfer calculations (Hoeflich & Khokhlov 1996; Nugent et al. 1997; Kromer et al. 2010; Woosley & Kasen 2011; Polin et al. 2018).

In particular, these models find that He shell double detonation events exhibit spectra that are strongly influenced by Fe-group line blanketing features from the overlying burned material, thus producing unusually red colors near peak light. These features remain generally inconsistent with the observed variety of Type Ia SNe for the minimum He shell masses that have been previously suggested to detonate the core ($\sim 0.05\,M_\odot$; as found in the initial simulations of Bildsten et al. 2007 and Fink et al. 2010). Several solutions to these discrepancies have been proposed, including possible differences in the composition of the burnt He shell (e.g. due to pollution of the initial He shell by C; Kromer et al. 2010). Alternatively, it has been suggested that the observed variety of Type Ia SNe could be produced from detonations of thin He shells with even lower masses ($\lesssim 0.01\,M_\odot$) that may still detonate the core (Shen & Moore 2014; Shen et al. 2018; Polin et al. 2018).

In this paper, we present observations of ZTF 18aaqeasu, a peculiar Type I SN that exhibits remarkable similarities to expected signatures of a He-shell double detonation on a white dwarf. Section 2 presents the observations of the transient. Section 3 presents a comparison of this source to known Type Ia SNe. Section 4 presents a comparison of the data to models of He shell detonations presented in Kromer et al. (2010) and a larger grid presented in Polin et al. (2018). We end with a discussion of the observations in the broader context of Type Ia SNe in Section 5. Calculations in this paper assume a ΛCDM cosmology with $H_0 = 70\,\mathrm{km\,s^{-1}\,Mpc^{-1}}$, $\Omega_M = 0.27$ and $\Omega_\Lambda = 0.73$ (Komatsu et al. 2011).

2. OBSERVATIONS

2.1. *Detection and classification*

On 2018 May 04.268[1] (MJD 58242.268), ZTF 18aaqeasu was first detected by the Zwicky Transient Facility (ZTF; Bellm et al. 2018; Graham et al. 2018) using the 48-inch Samuel Oschin Telescope (P48) at Palomar Observatory in a nightly cadence experiment. This detection was at an r-band magnitude of $\approx 20.57\,\mathrm{mag}$ and J2000 coordinates $\alpha = 12^\mathrm{h}23^\mathrm{m}21.57^\mathrm{s}$, $\delta = 46°36'08.3''$. The source was not detected on 2018 April 25.198 (MJD 58233.198; 9.07 days before first detection) up to a limiting magnitude of $r \geq 20.11\,\mathrm{mag}$.

On 2018 May 7, ZTF 18aaqeasu met machine-learning thresholds and was flagged by a science program filter on the GROWTH Marshal (Kasliwal et al. 2018) that is designed to look for transients in the vicinity of nearby galaxies. ZTF 18aaqeasu was detected in the outskirts of an elliptical galaxy at a redshift of $z = 0.066$ (Figure 1). On 2018 May 8.19, we obtained the first spectrum, which exhibited blue continua with broad absorption features below 5000 Å (Section 2.3). On 2018 May 14.34, a subsequent spectrum exhibited prominent Si II absorption features as well as a sharp cut-off in flux below 5000 Å. As such, due to the strong Si II features and absence of any H features, we tentatively classified the transient as a peculiar Type Ia SN (see Filippenko 1997 for a review).

On 2018 May 22.42, the transient was independently detected at 18.9 mag by the ATLAS survey (Tonry et al. 2018) as ATLAS18pqq. On 2018 May 25, ATLAS reported this event to the Transient Name Server (TNS) and the event was given the IAU name AT 2018byg. On 2018 Nov 19, we reported the spectroscopic classification and it was re-named as SN 2018byg. Hereafter, we refer to the source by the name ZTF 18aaqeasu.

---

[1] UT times are used throughout the paper

2.2. *Optical Photometry*

We obtained r-band photometry of ZTF 18aaqeasu with the ZTF camera, along with gri-band photometry with the Spectral Energy Distribution Machine (SEDM; Blagorodnova et al. 2018) mounted on the automated 60-inch telescope (P60; Cenko et al. 2006) at Palomar observatory. The P48 images were reduced with the Zwicky Transient Facility Image Differencing pipeline (Masci et al. 2018), which performs host subtracted point spread function (PSF) photometry, while the P60 images were reduced using the pipeline described in Fremling et al. (2016). We also obtained one epoch of g-band imaging with the Wafer Scale Imager for Prime (WASP) instrument mounted on the 200-inch Hale telescope at Palomar observatory on 09 June 2018. These images were reduced with a custom-developed imaging pipeline based in `python`.

We correct all our photometry for galactic extinction for $A_V = 0.032$ mag from the maps of Schlafly & Finkbeiner (2011). We do not correct for any additional host extinction due to the offset location of the transient, and the absence of any Na I D absorption at the host redshift in our spectra. We show the multi-color light curves (magnitudes are in the AB system) of ZTF 18aaqeasu in Figure 1. For all subsequent discussion, we refer phases with respect to the maximum of the r-band light curve.

2.3. *Optical spectroscopy*

We obtained optical spectroscopic follow-up of the transient starting from ≈ -10 d to $\approx +53$ d after r-band peak using the Double Beam Spectrograph (DBSP; on 2018 May 08, 2018 May 17 and 2018 June 08) on the 200-inch Hale telescope (Oke & Gunn 1982), the Low Resolution Imaging Spectrograph (LRIS; on 2018 May 14, 2018 June 17 and 2018 July 13) on the Keck-I telescope (Oke et al. 1995), the SEDM (on 2018 May 28), and the DeVeny spectrograph (on 2018 May 31) on the Discovery Channel Telescope (Bida et al. 2014). We present our sequence of spectra in Figure 2. All spectra will be made publicly available via the WISeREP repository (Yaron & Gal-Yam 2012).

2.4. *NIR photometry and spectroscopy*

We obtained Near Infrared (NIR) JHK band imaging of the transient using the Multi-Object Spectrometer for Infrared Exploration (MOSFIRE; McLean et al. 2012) on the Keck-I telescope on 2018 June 03 (≈ 13 days after r-band peak). Dithered science exposures of the target field were obtained in each band for a total exposure time of 231 s, 192 s and 128 s in J, H and K_s bands respectively. The images were reduced using a custom-

built `python`-based imaging pipeline, and the transient was detected in all three filters. We measure Vega magnitudes of $J = 19.92 \pm 0.10$ mag, $H = 19.70 \pm 0.25$ mag and $K_s = 19.29 \pm 0.22$ mag. We also obtained a Y-band (9700–11100 Å) spectrum of the transient with MOSFIRE on 2018 June 03, for a total integration time of 720 s. The spectra were reduced with the MOSFIRE Data Reduction Pipeline, and are shown in Figure 2.

2.5. *Swift XRT observations*

We obtained X-ray follow-up of the transient with the Swift X-ray telescope (XRT; Burrows et al. 2005) on the Neil Gehrels Swift Observatory (Swift; Gehrels et al. 2004). The Swift observatory observed the location of the transient on 2018 May 27 (≈ 8 days after r-band peak) for a total exposure time of 3.8 ks. No source was detected at the location of the transient down to a 3σ limiting flux of 3.5×10^{-3} count s^{-1}, corresponding to a 0.3–10 keV flux of 1.2×10^{-13} ergs cm^{-2} s^{-1}. This corresponds to an X-ray luminosity of $\lesssim 1.3 \times 10^{42}$ ergs s^{-1} at the distance of the host galaxy for a photon index of $\Gamma = 2$. In the same observation, no source was detected with the Ultraviolet Optical telescope (UVOT; Roming et al. 2005) in the UVW2 filter, down to a 5σ limiting AB magnitude of 22.40.

3. ANALYSIS

3.1. *Photometric properties*

The transient exhibited a light curve fainter than the normal Type Ia SNe, but similar to the subluminous 1991bg-like events. To this end, we compare the photometric evolution of ZTF 18aaqeasu to the light curves of the normal Type Ia SNe 2011fe (Nugent et al. 2011) and SN 2015F (Cartier et al. 2017), as well as the subluminous (SN 1991bg-like) Type Ia SNe 2005ke, 2005bl and 2006mr (Contreras et al. 2010), in Figure 3 (data taken from the Open Supernova Catalog; Guillochon et al. 2017). The source exhibited an initial fast rise (at < -10 days from peak) of ≈ 0.4 mag day^{-1} similar to the normal Type Ia SNe but subsequently slowed in its rise transitioning to a sub-luminous SN Ia light curve.

By fitting the peak of the light curve with a low order polynomial, we find a best-fit peak time in r-band of MJD 58258.49, and a peak absolute magnitude of $M_r = -18.27 \pm 0.04$ mag. Integrating the total flux in the optical spectrum of the source near peak light (at ≈ -2 days; after performing an absolute calibration with respect to r-band photometry), we find a lower limit on the peak luminosity of $\approx 2.4 \times 10^{42}$ ergs s^{-1}. Using Arnett's law for the synthesized ^{56}Ni mass (Ar-
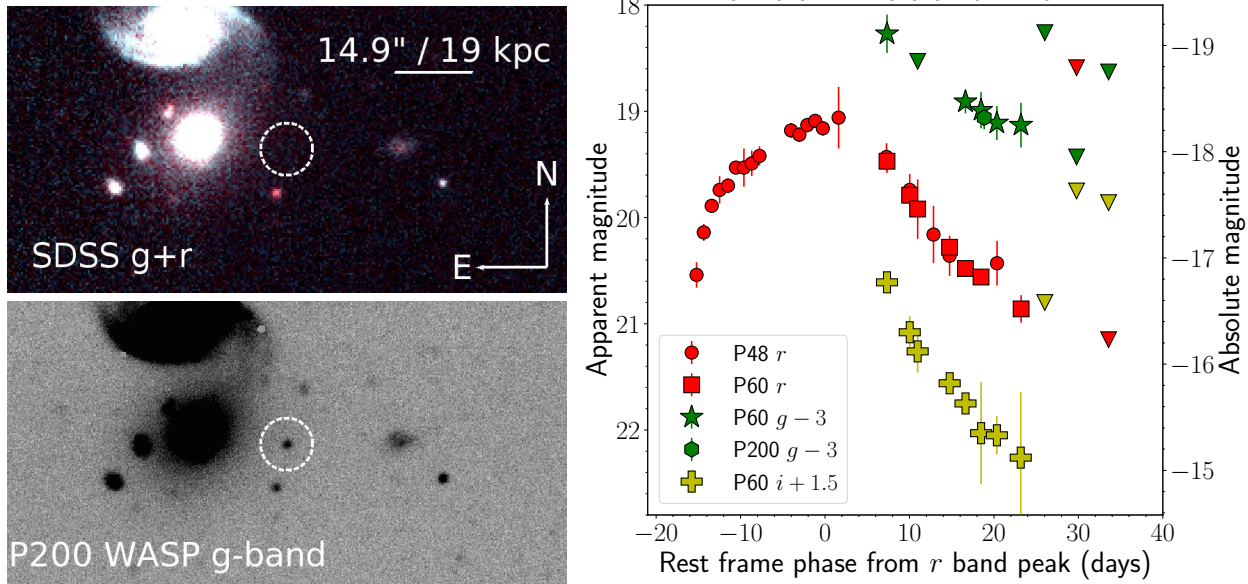
Figure 1. (Left) Detection field and host galaxy of ZTF 18aaqeasu. The top panel is an archival SDSS image of the region while the lower panel shows an image taken with WASP on P200. The location of the transient is marked with the white circle - it is at a projected offset of $\approx 17.2''$ corresponding to a physical projected distance of 21.9 kpc at the host galaxy redshift. (Right) Multi-color light curves of ZTF 18aaqeasu. The inverted triangles are upper limits. The epochs of spectroscopy are marked with 'S' on the top axis.

nett et al. 1985), we use the peak luminosity to find ^{56}Ni mass $\gtrsim 0.11\,\mathrm{M}_\odot$.

Although we do not have multi-color photometric coverage before the peak of the r-band light curve, we use our well sampled sequence of spectra to construct pre-peak color curves for the transient. We constructed $g-r$ and $r-i$ color curves of the transient by performing synthetic photometry on the spectra, while adding a 10% uncertainty on the measurements to account for potential inaccuracies in flux calibration. The colors derived from spectroscopy are consistent with contemporaneous multi-color photometry at epochs after peak light. The color evolution is shown in in Figure 3. Comparing the color curves to the other Type Ia SNe, we find that while the $r - i$ color evolution is similar to the subluminous Type Ia SNe in the light curve comparison sample, the $g - r$ color of the transient ($g - r \approx 2$ at peak light) is ≈ 1.5 mag redder near peak light than all the Type Ia SNe in the comparison sample.

3.2. *Spectroscopic properties*

We show a comparison of the pre-maximum and post-maximum spectroscopic evolution of ZTF 18aaqeasu with other Type Ia SNe in Figure 4. The earliest spectrum of the source was obtained ≈ 10 days before r-band peak and exhibits blue continua with broad absorption features blue-wards of $\approx 5500\,\text{Å}$, notably without any Si II features that are characteristic of normal and

sub-luminous Type Ia SNe at similar phases (Figure 4). However, there are several similarities between this spectrum and SN 1991T at a similar phase, particularly in the absence of a Si II feature and the presence of broad absorption features of Ti II and Fe group elements near $4100\,\text{Å}$ and $4700\,\text{Å}$ respectively. This spectrum also shows signatures of an absorption feature in the Ca II NIR triplet.

Subsequent spectra taken at ≈ 5 and ≈ 2 days before r-band peak exhibit the hallmark Si II absorption features found in Type Ia SNe near peak light. Using the minimum of the Si II P-Cygni profile, we measure a photospheric velocity of $\approx 10,500\,\mathrm{km\,s^{-1}}$. However, the bluer parts of the spectra exhibit unusually strong line blanketing features leading to nearly complete absorption of flux blue-wards of $5000\,\text{Å}$. Comparing with the subluminous Type Ia SN 1991bg at a similar phase, we attribute this absorption to complete line blanketing by Fe group elements and Ti II. To our knowledge, such strong line blanketing features (and consequent red $g-r$ colors) have never been previously seen in any variant of a Type Ia SN at peak light. The Ca II triplet also develops into a deep, high velocity ($\approx 25,000\,\mathrm{km\,s^{-1}}$) absorption feature at 7500–8500 Å near peak.

Post-maximum spectra starting from ≈ 10 days after peak (Figure 4) begin to develop broad emission features suggesting a transition to the optically thin phase.
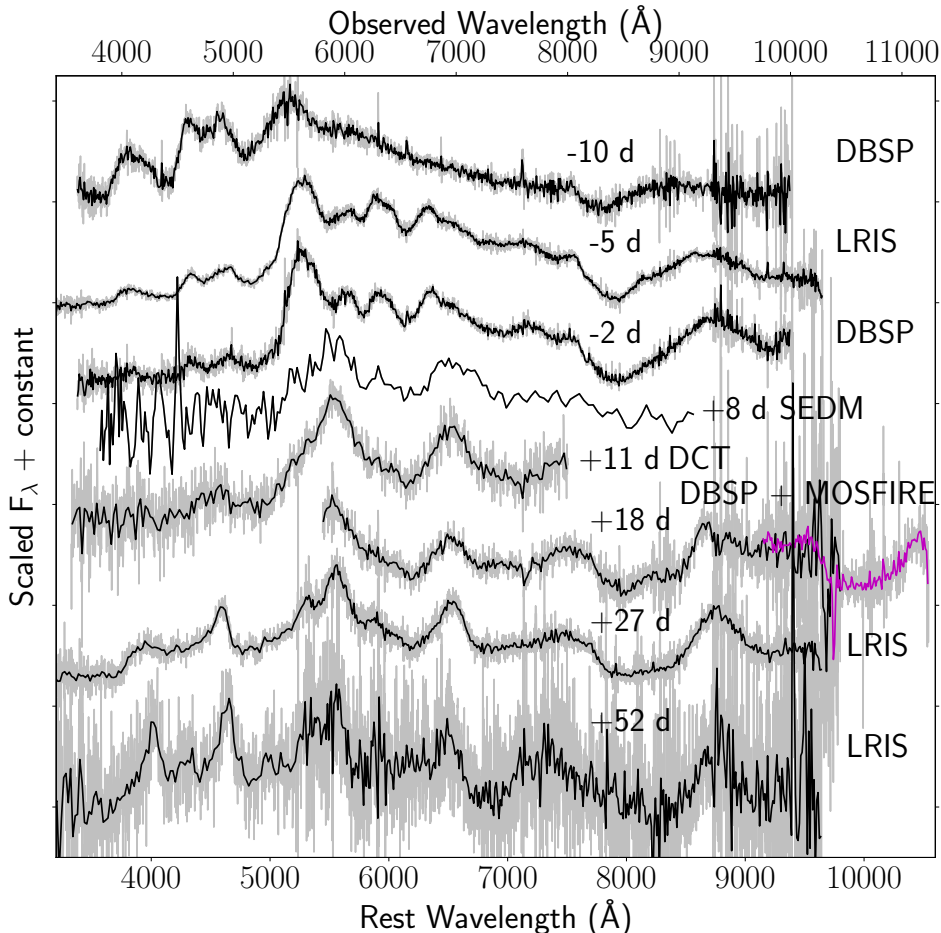
Figure 2. Spectroscopic sequence of ZTF 18aaqeasu. Phases with respect to r-band peak and instruments used are indicated next to each spectrum. The black lines are binned from the raw spectra shown in gray lines. The magenta line at +18 days indicates the only NIR spectrum of the source in Y band from MOSFIRE.

The only NIR spectrum taken at +18 days exhibits a deep absorption feature at $\approx 9950\,\text{Å}$. If associated with He I at $1.083\,\mu$m, the corresponding absorption velocity would be $\approx 26{,}000\,\text{km}\,\text{s}^{-1}$. Spectra obtained at ≈ 27 and ≈ 52 days after peak are similar to the Type Ia SN 1991bg at similar phases, and exhibit emission lines of Fe group elements, Ti II and Ca II. The late-time similarities and Fe-group dominated nucleosynthesis suggest a thermonuclear origin of the explosion, consistent with ZTF 18aaqeasu representing an unusual variant of a Type Ia-like SN. However, the peculiar spectral features observed at peak light are unique to ZTF 18aaqeasu and warrant further inspection with respect to a possible explosion mechanism.

4. MODEL COMPARISONS

The strong line blanketing features of Fe group elements observed in the peak spectra suggest that the outer layers of the ejecta are unusually rich in Fe group elements. The presence of such radioactive material in

the outer ejecta would also be consistent with the fast rise observed in the early light curve (Piro & Nakar 2014), and is a hallmark signature of the decay of radioactive elements in the outermost ejecta (primarily ^{48}Cr and ^{52}Fe with half-lives of 0.90 days and 0.35 days respectively) for an explosion powered by a He shell detonation (e.g. Nugent et al. 1997; Kromer et al. 2010; Polin et al. 2018). This scenario would naturally explain the high velocity Ca II features observed near peak light, as a known He detonation product in the outer layers of the ejecta (Fink et al. 2010; Kromer et al. 2010; Moore et al. 2013).

We thus compare the properties of ZTF 18aaqeasu to simulations in the grid of models of He shell double detonations in Kromer et al. (2010), who modeled the observable signatures for the minimum shell masses found in Bildsten et al. (2007). We show a comparison of the r-band light curve, as well as the $g-r$ and $r-i$ colors of ZTF 18aaqeasu to their angle averaged light curves
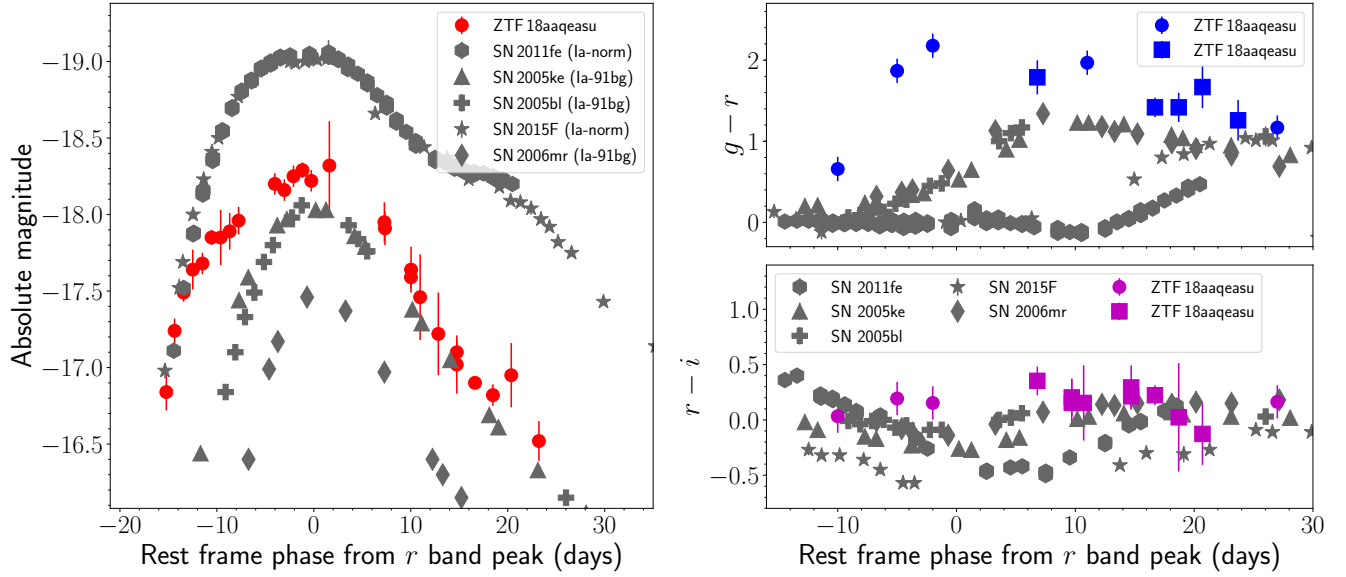
Figure 3. (Left) Comparison of the r-band light curve of ZTF 18aaqeasu to other normal and sub-luminous Type Ia SNe. (Right) Comparison of the $g-r$ and $r-i$ color evolution of ZTF 18aaqeasu (circles are colors derived from spectra while squares denote colors from photometry) to the same sample of SNe as in the left panel.
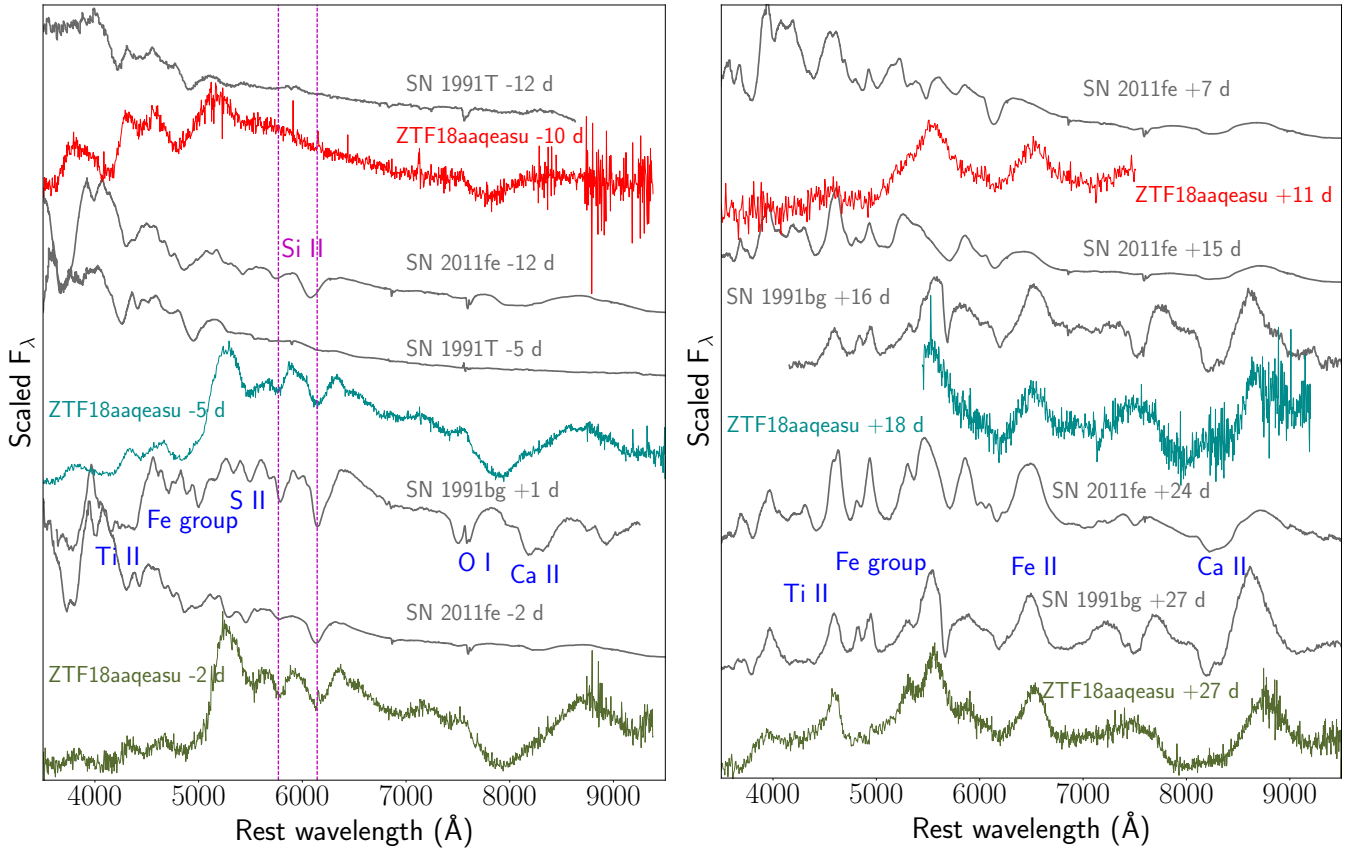
Figure 4. Comparison of the pre-maximum (left) and post-maximum (right) spectra of ZTF18aaqeasu to the normal Type Ia SN 2011fe (Maguire et al. 2014), the over-luminous SN 1991T (Filippenko et al. 1992a) and the sub-luminous SN 1991bg (Filippenko et al. 1992b). The magenta dashed lines in the left panel indicate Si II lines at a velocity of 10,000 km s^{-1}. Prominent emission / absorption features are marked in both panels. Spectroscopic data for the comparison SNe were obtained from the WISEReP repository (Yaron & Gal-Yam 2012).

in Figure 5 (dashed lines). As shown, their lowest core   mass model (with a WD core mass of $0.81\,M_\odot$; their
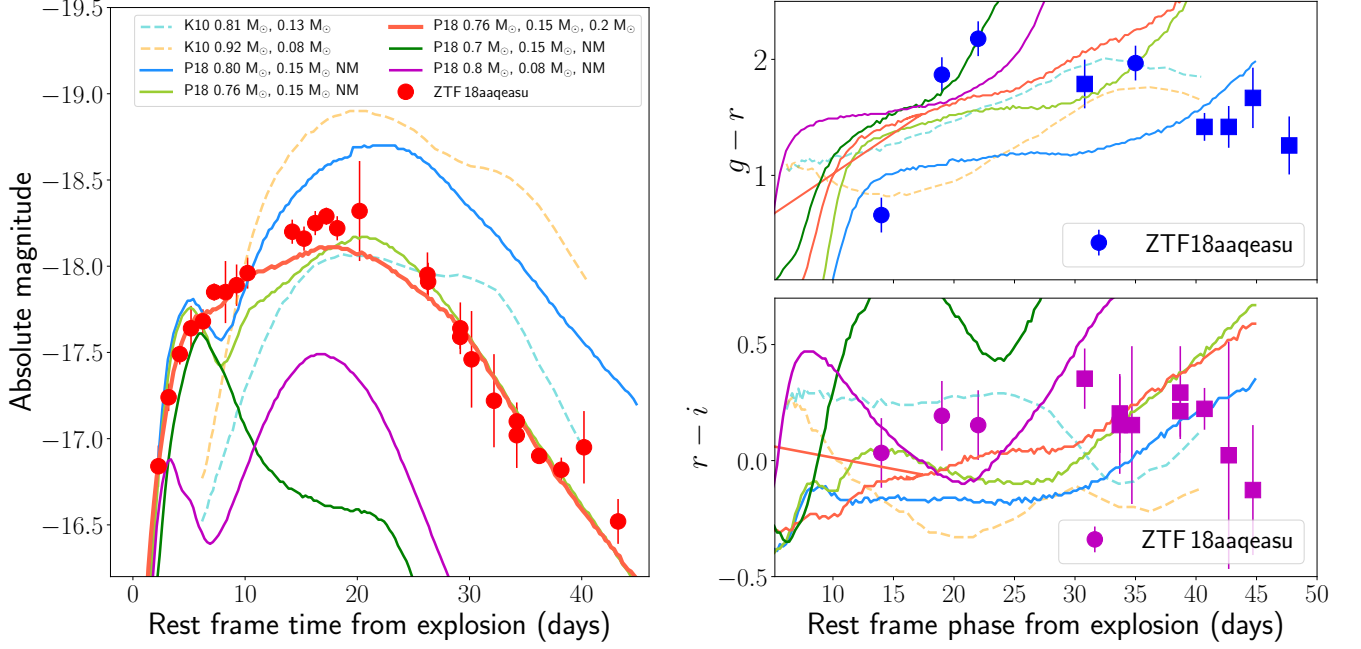
Figure 5. Comparison of the photometric evolution of ZTF 18aaqeasu with that of the He shell double detonation models in Kromer et al. (2010) (K10; dashed lines) and Polin et al. (2018) (P18; solid lines). The model parameters are indicated in the legend as (WD mass, shell mass, mixing length), and where NM stands for No Mixing. The left panel shows the r-band evolution while the right panels show the $g - r$ and $r - i$ color evolution with the same color schemes for the models. On the right panel, circles denote colors derived from the spectra while squares denote colors derived from photometry.
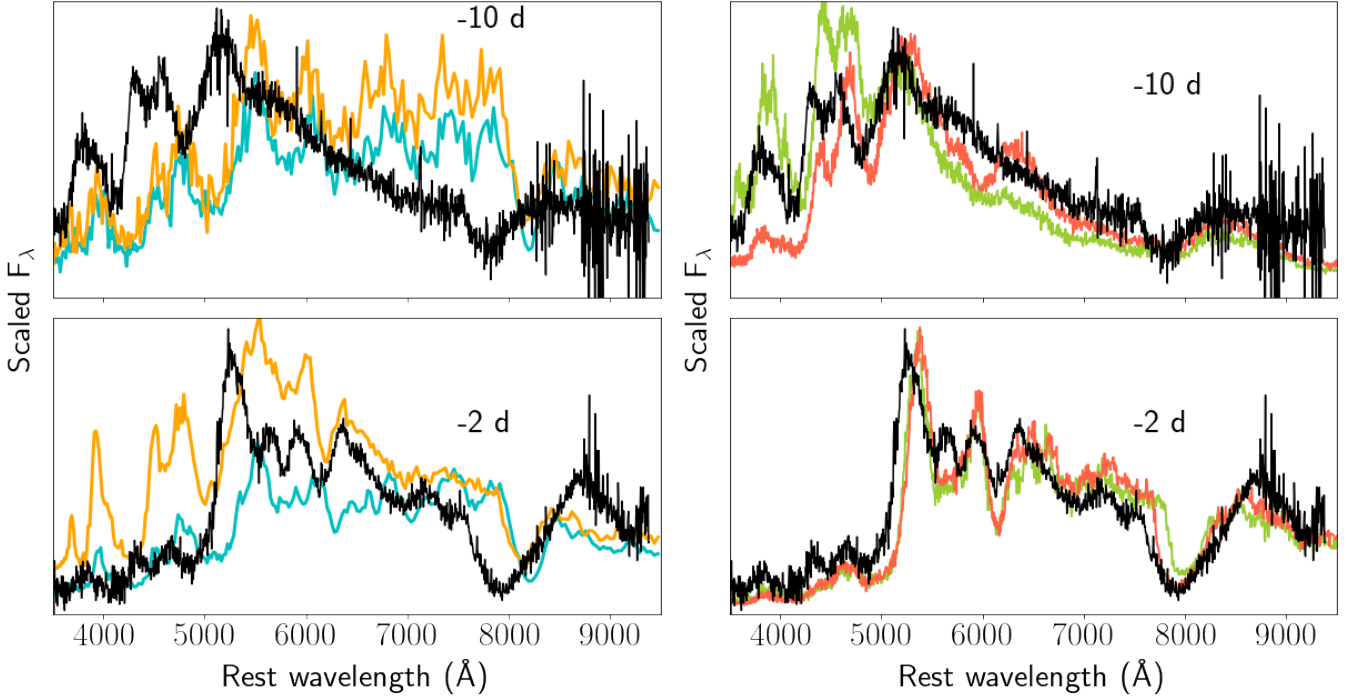
Figure 6. Comparison of the spectra of ZTF 18aaqeasu at and before peak light (shown as black lines) to models of He shell double detonations from Kromer et al. (2010) (left; for the two models shown in the light curve comparison) and Polin et al. (2018) (right; for two cases of ejecta mixing with the best fit WD and shell mass from the light curves). In both panels, the epochs of spectroscopic comparison are indicated according to the phase of the light curve (days from r-band peak), and the model spectra have the same color scheme as in Figure 5.

Model 1) shows similarities to the data both in terms of   absolute luminosity and red colors near peak, although

the light curve shapes are not well matched. The larger luminosity of models involving higher mass WDs (yellow dashed lines) disfavor WD masses $\gtrsim 0.8\,M_\odot$.

We also compare the light curves to the larger grid of shell and WD masses presented in the simulations of Polin et al. (2018), including additional simulations performed to match the data (using the radiative transfer code SEDONA; Kasen et al. 2006), as solid lines in Figure 5. For the additional simulations, we model the explosion of a 50% carbon + 50% oxygen WD with an isentropic helium shell. The hydrodynamics and nuclear processes are modeled from the helium ignition until the ejecta reaches homologous expansion using the compressible hydrodynamics code Castro (Almgren et al. 2010). Once the explosion reached homology radiative transport calculations are performed using SEDONA to produce light curves and spectra from the ejecta.

Since the early rise in the light curve is powered by the radioactive He shell detonation products (^{48}Cr and ^{52}Fe), we can constrain the mass of the shell. We note that a model involving a fixed WD mass of $0.8\,M_\odot$ and a shell of $0.15\,M_\odot$ shell reasonably reproduces the early rise, while the same WD with a smaller $0.08\,M_\odot$ shell under-predicts the r-band luminosity on the early rise. We then constrain the WD mass to be between 0.7 and $0.8\,M_\odot$ by noting that models involving a $0.8\,M_\odot$ WD and $0.7\,M_\odot$ WD (each with a $0.15\,M_\odot$ shell) have a higher and lower peak luminosity than ZTF 18aaqeasu respectively. With these constraints, we find that a model with a $0.76\,M_\odot$ WD and a $0.15\,M_\odot$ shell reproduces the overall r-band evolution. The corresponding synthesized ^{56}Ni mass is $0.18\,M_\odot$.

The light curves in these models also exhibit an early peak and decline, arising from the decay of radioactive material in the outer ejecta and the assumption of no mixing. Although we do observe signatures of a fast rising early peak, we do not have evidence of a decline as in the models, suggesting a possible influence of mixing in the ejecta. Hence, we also show an additional model with the best-fit WD mass and shell mass, but with ejecta mixed across a zone of $0.18\,M_\odot$ that is applied before performing the radiative transport. This model reproduces the early-time rise and the overall light curve. Although the red colors of the source near peak light are also well reproduced, the models become redder with time much faster than observed in the data. These discrepancies likely arise due to assumptions of local thermodynamic equilibrium (LTE) in SEDONA, which break down as the source transitions to the optically thin nebular phase at ≈ 20 days after peak light.

We also compare the spectroscopic properties of ZTF 18aaqeasu to double detonation models in Figure 6. While there are several similarities between the model spectra of Kromer et al. (2010) and spectra near peak light (≈ 2 days before peak light), including the strong line blanketing features below 5000 Å and deep Ca II absorption features, their limited grid of models does not correctly reproduce the line velocities and strengths of the prominent Si II and Ca II absorption features. Additionally, these models exhibit strong line blanketing features below 5000 Å and Si II absorption even at ≈ 10 days before peak, unlike the observed properties of this event where Si II lines appear only near peak light.

Comparing to the best-fit light curve model from Polin et al. (2018), we find a better match to the observed spectra both before and at peak light (Figure 6). In the case of the early spectra (≈ 10 days before peak), the models exhibit blue continua in the unmixed case similar to the data, although the absorption features become more prominent in the case of mixed ejecta as expected. The peak light spectra (≈ 2 days before peak) are well reproduced both in terms of line velocities and strengths, and are not appreciably affected by mixing in the ejecta. Taken together, we find that a model involving the detonation of a $\approx 0.15\,M_\odot$ He shell on a $\approx 0.75\,M_\odot$ WD reproduces the observed signatures of the event after including mixing of $\approx 0.2\,M_\odot$ in the outer ejecta.

5. DISCUSSION AND CONCLUSION

In this paper, we have presented observations of the transient ZTF 18aaqeasu, and have shown it to be a unique supernova. While its photometric and nucleosynthetic properties share several similarities to subluminous Type Ia SNe, its peak photospheric spectra are marked by extremely strong line blanketing features and red colors, unlike any previously observed Type Ia SN. By comparing the data to a grid of models, we show that the observed properties can be well explained by the detonation of a massive ($\approx 0.15\,M_\odot$) He shell on a sub-Chandrasekhar mass ($\approx 0.75\,M_\odot$) white dwarf. In particular, it is important to note that the He shell mass inferred is much larger than the thin He shells required to explain the properties of the broader population of Type Ia SNe ($\lesssim 0.01\,M_\odot$; Kromer et al. 2010; Sim et al. 2010; Shen et al. 2018; Polin et al. 2018).

The inferred shell and core masses are consistent with what is predicted in the well studied He burning star

donor scenario of a $0.48\,\mathrm{M_\odot}$ sdB star losing matter to a C/O WD (Nomoto 1982a; Woosley & Weaver 1994; Woosley & Kasen 2011). While much of the early work assumed a constant accretion rate, more recent calculations (Brooks et al. 2015; Bauer et al. 2017) have self consistently calculated the evolution of the donor with mass loss and a self-consistent varying accretion rate. The properties inferred for ZTF 18aaqeasu are remarkably close to the recent calculation of Bauer et al. (2017) for the evolution of the known sdB + WD binary CD $-30°11223$ (Geier et al. 2013), with Bauer et al. (2017) finding a He shell mass of $0.16\,\mathrm{M_\odot}$ on the initial WD of mass $0.76\,\mathrm{M_\odot}$ at the time of detonation. As this is the forward evolution of a known system, its possible to say that CD $-30°11223$ is indeed an example of the progenitor of ZTF 18aaqeasu-like events.

The relatively luminous and slow evolving light curve of ZTF 18aaqeasu (compared to e.g. SN 1991bg-like events) suggests that similar events should be easily detectable in a reasonably large volume of the local universe (out to $z \approx 0.1$ for a limiting magnitude of $r = 20.5\,\mathrm{mag}$). However, no such event has been reported in previous studies of large samples of thermonuclear SNe (e.g., Hicken et al. 2009; Maguire et al. 2014; Krisciunas et al. 2017; Scolnic et al. 2018). To date, tentative evidence for only one other example of a relatively thin He shell detonation has been presented in Jiang et al. (2017) (see also Polin et al. 2018), although their modeling implies a more massive WD with a smaller He shell than is needed to explain ZTF 18aaqeasu. Thus, ZTF 18aaqeasu being the first of its kind suggests that massive He shell double detonations must be intrinsically rare in the population of thermonuclear SNe.

REFERENCES

Almgren, A. S., Beckner, V. E., Bell, J. B., et al. 2010, ApJ, 715, 1221

Arnett, W. D., Branch, D., & Wheeler, J. C. 1985, Nature, 314, 337

Bauer, E. B., Schwab, J., & Bildsten, L. 2017, ApJ, 845, 97

Bellm, E. C., et al. 2018, submitted to PASP

Bida, T. A., Dunham, E. W., Massey, P., & Roe, H. G. 2014, in Proc. SPIE, Vol. 9147, Ground-based and Airborne Instrumentation for Astronomy V, 91472N

Bildsten, L., Shen, K. J., Weinberg, N. N., & Nelemans, G. 2007, ApJL, 662, L95

Blagorodnova, N., Neill, J. D., Walters, R., et al. 2018, PASP, 130, 035003

Brooks, J., Bildsten, L., Marchant, P., & Paxton, B. 2015, ApJ, 807, 74

Burrows, D. N., Hill, J. E., Nousek, J. A., et al. 2005, Space Science Reviews, 120, 165

Cartier, R., Sullivan, M., Firth, R. E., et al. 2017, MNRAS, 464, 4476

Cenko, S. B., Fox, D. B., Moon, D.-S., et al. 2006, PASP, 118, 1396

Contreras, C., Hamuy, M., Phillips, M. M., et al. 2010, AJ, 139, 519

Filippenko, A. V. 1997, ARA&A, 35, 309

Filippenko, A. V., Richmond, M. W., Matheson, T., et al. 1992a, ApJL, 384, L15

Filippenko, A. V., Richmond, M. W., Branch, D., et al. 1992b, AJ, 104, 1543

Fink, M., Hillebrandt, W., & Röpke, F. K. 2007, A&A, 476, 1133

Fink, M., Röpke, F. K., Hillebrandt, W., et al. 2010, A&A, 514, A53

Fremling, C., Sollerman, J., Taddia, F., et al. 2016, A & A, 593, A68

Gehrels, N., Chincarini, G., Giommi, P., et al. 2004, ApJ, 611, 1005

Geier, S., Marsh, T. R., Wang, B., et al. 2013, A&A, 554, A54

Graham, M. J., et al. 2018, submitted to PASP

Guillochon, J., Parrent, J., Kelley, L. Z., & Margutti, R. 2017, ApJ, 835, 64

Hicken, M., Challis, P., Jha, S., et al. 2009, ApJ, 700, 331

Hoeflich, P., & Khokhlov, A. 1996, ApJ, 457, 500

Jiang, J.-A., Doi, M., Maeda, K., et al. 2017, Nature, 550, 80

Kasen, D., Thomas, R. C., & Nugent, P. 2006, ApJ, 651, 366

Kasliwal, M., et al. 2018, submitted to PASP

Komatsu, E., Smith, K. M., Dunkley, J., et al. 2011, ApJS, 192, 18

Krisciunas, K., Contreras, C., Burns, C. R., et al. 2017, AJ, 154, 211

Kromer, M., Sim, S. A., Fink, M., et al. 2010, ApJ, 719, 1067

Livne, E., & Arnett, D. 1995, ApJ, 452, 62

Maguire, K., Sullivan, M., Pan, Y.-C., et al. 2014, MNRAS, 444, 3258

Masci, F. J., Laher, R. R., Rusholme, B., Shupe, D. L., et al. 2018, submitted to PASP

McLean, I. S., Steidel, C. C., Epps, H. W., et al. 2012, in Proc. SPIE, Vol. 8446, Ground-based and Airborne Instrumentation for Astronomy IV, 84460J

Moore, K., Townsley, D. M., & Bildsten, L. 2013, ApJ, 776, 97

Nomoto, K. 1980, SSRv, 27, 563

—. 1982a, ApJ, 253, 798

—. 1982b, ApJ, 257, 780

Nugent, P., Baron, E., Branch, D., Fisher, A., & Hauschildt, P. H. 1997, ApJ, 485, 812

Nugent, P. E., Sullivan, M., Cenko, S. B., et al. 2011, Nature, 480, 344

Oke, J. B., & Gunn, J. E. 1982, PASP, 94, 586

Oke, J. B., Cohen, J. G., Carr, M., et al. 1995, PASP, 107, 375

Patterson, M. T., et al. 2018, in Press

Piro, A. L., & Nakar, E. 2014, ApJ, 784, 85

Polin, A., Nugent, P., & Kasen, D. 2018, ArXiv e-prints, arXiv:1811.07127

Roming, P. W. A., Kennedy, T. E., Mason, K. O., et al. 2005, Space Science Reviews, 120, 95

Schlafly, E. F., & Finkbeiner, D. P. 2011, ApJ, 737, 103

Scolnic, D. M., Jones, D. O., Rest, A., et al. 2018, ApJ, 859, 101

Shen, K. J., & Bildsten, L. 2014, ApJ, 785, 61

Shen, K. J., Kasen, D., Miles, B. J., & Townsley, D. M. 2018, ApJ, 854, 52

Shen, K. J., Kasen, D., Weinberg, N. N., Bildsten, L., & Scannapieco, E. 2010, ApJ, 715, 767

Shen, K. J., & Moore, K. 2014, ApJ, 797, 46

Sim, S. A., Röpke, F. K., Hillebrandt, W., et al. 2010, ApJL, 714, L52

Tonry, J. L., Denneau, L., Heinze, A. N., et al. 2018, PASP, 130, 064505

Woosley, S. E., & Kasen, D. 2011, ApJ, 734, 38

Woosley, S. E., Taam, R. E., & Weaver, T. A. 1986, ApJ, 301, 601

Woosley, S. E., & Weaver, T. A. 1994, ApJ, 423, 371

Yaron, O., & Gal-Yam, A. 2012, PASP, 124, 668